

## EFFECTS OF THE BOUNDARY LAYER TRANSITION ON THE GLOBAL AERODYNAMIC COEFFICIENTS

Gustavo L. O. Halila\*, Alexandre P. Antunes\*, Ricardo G. da Silva<sup>†</sup>, João Luiz F. Azevedo<sup>†</sup>

\* Embraer, Research and Development Branch, São José dos Campos, SP, Brazil

<sup>†</sup> Instituto de Aeronáutica e Espaço, São José dos Campos, SP, Brazil

**Keywords:** *Boundary Layer Transition, CFD, High-Lift Configuration, Aerodynamic Design*

### Abstract

The numerical results for global aerodynamic coefficients and overall flow topology obtained with the Langtry-Menter  $\gamma - Re_{\theta}$  transitional model are compared with previous results obtained with Sparlat-Allmaras, Menter SST and cubic  $k - \epsilon$  turbulence models. The numerical simulations are performed using configuration “one” from the 1st AIAA CFD High-Lift Prediction Workshop as the testbed, which is a trapezoidal wing with a 30 deg. slat deflection and a full-span flap with 25 deg. deflection. The numerical simulations are accomplished with the CFD++ solver considering the Reynolds-averaged Navier-Stokes formulation (RANS). The hexahedral mesh approach is here considered and the results are obtained for a hexahedral mesh with 22.8 million cells. Experimental data from NASA Langley 14 by 22-foot Subsonic Wind Tunnel (SWT) provide the global aerodynamic information for the verification of the obtained numerical results.

### 1 Introduction

In the present paper the numerical simulations are performed with the CFD++ commercial package [1] considering the Langtry-Menter  $\gamma - Re_{\theta}$  transition model [2]. The simulations are performed over configuration “one” from the 1st AIAA CFD High-Lift Prediction Workshop. Such high-lift configuration presents a 30 deg. slat deflection and a full-span flap with 25 deg. deflection. The numerical simulations are performed using a hex-

ahedral mesh with 22.8 million cells. The flight condition is defined by a Reynolds number of 4.3 million, based on the mean aerodynamic chord, and a freestream Mach number of 0.20.

The results obtained for the Langtry-Menter  $\gamma - Re_{\theta}$  transition model are compared with results previously produced by the authors [3] with the cubic  $k - \epsilon$ , the Sparlat-Allmaras [4] and the Menter SST [5] turbulence models. It is important to mention that all the results depicted here were obtained with the same 22.8 million cells hexahedral mesh. The comparisons are accomplished not only for the global aerodynamic coefficients but also for the flow pattern over the aerodynamic components.

In Fig. 1 one can see the blocking concept, typical of the hexahedral mesh methodology, and the resulting surface mesh generated by the use of this methodology. This concept consists in attributing the edges of the blocks to the surface and boundaries of the geometry, whenever the block is close enough of the geometry. These blocks are responsible for the generation of the surface mesh and the volumetric mesh close to the surface. Those blocks that are in regions far from the geometry are only responsible for representing the volumetric mesh. Their edges are attached to the mesh supporting lines. The process just described is the usual approach adopted by the ICEM-CFD [6] solver for hexahedral mesh generation.

The motivation for such investigation lies on the fact that very few numerical results in the 1st AIAA CFD High-Lift Prediction Workshop

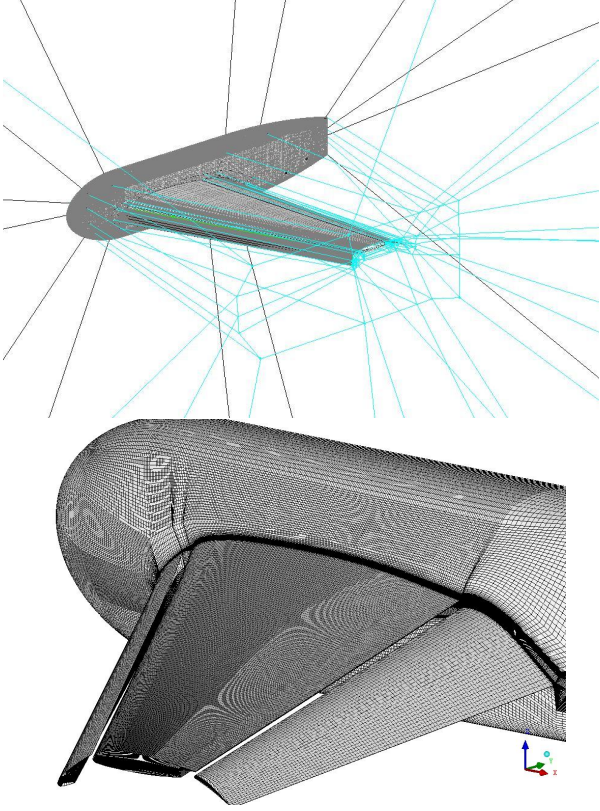


**Fig. 1** Hexahedral mesh blocks and surface mesh for configuration *one*.

have considered the boundary layer transition in the simulations process for configuration “one”. The summary of the Workshop suggests that the adoption of a boundary layer transition modeling can yield a better adherence with the experimental data.

The Langtry-Menter model allows for the inclusion of transitional effects based on local properties which avoids the excessive increase in computational costs due to the need to integrate the flow properties up to the edge of the boundary layer. This model can be categorized as a Local Correlation-Based Transition Model (LCTM) which is a term used in order to distinguish the present model formulation from a more complex physics-based transport modeling.

## 2 Transition Model

The Langtry-Menter (LM) [2] correlation-based transition model is composed of two additional transport equations, besides the equations for the

SST turbulence model [7]. These equations are used to estimate transition onset and the extent region. This is possible due to the combination of the strain-rate Reynolds number with experimental transition correlations. In addition, viscous sublayer damping and transition predictions are independent. The first transport equation based on the intermittency reads

$$\begin{aligned} \frac{\partial(\rho\gamma)}{\partial t} + \frac{\partial(\rho u_j \gamma)}{\partial x_j} &= P_\gamma - E_\gamma \\ &+ \frac{\partial}{\partial x_j} \left[ \left( \mu + \frac{\mu_t}{\sigma_f} \right) \frac{\partial \gamma}{\partial x_j} \right] \end{aligned} \quad (1)$$

The intermittency equation allows for the estimation of the extension of the transition region since the intermittency represents the probability of a fluid cell to be turbulent. Transition onset, on the other hand, is triggered by the momentum thickness Reynolds number transport equation which can be written as

$$\begin{aligned} \frac{\partial(\rho \tilde{R}e_{\theta t})}{\partial t} + \frac{\partial(\rho u_j \tilde{R}e_{\theta t})}{\partial x_j} &= P_{\theta t} \\ &+ \frac{\partial}{\partial x_j} \left[ \sigma_{\theta t} (\mu + \mu_t) \frac{\partial \tilde{R}e_{\theta t}}{\partial x_j} \right] \end{aligned} \quad (2)$$

The empirical correlations that complete the model can be found in the literature [2]. The interaction between the transition model and the SST turbulence model is performed by a modified kinetic energy production term,  $\tilde{P}_k$ , as

$$\begin{aligned} \frac{\partial(\rho k)}{\partial t} + \frac{\partial(\rho u_j k)}{\partial x_j} &= \tilde{P}_k - \tilde{D}_k \\ &+ \frac{\partial}{\partial x_j} \left[ (\mu + \sigma_k \mu_t) \frac{\partial k}{\partial x_j} \right] \end{aligned} \quad (3)$$

$$\tilde{P}_k = \gamma_{\text{eff}} P_k \quad (4)$$

where  $\gamma_{\text{eff}}$  is introduced in order to also include separation effects into the formulation. A very detailed description of the transition model can be found in Ref. [8].

## 3 Numerical Results

The numerical results are obtained using the Reynolds-averaged Navier-Stokes equations

(RANS). The spatial discretization adopted is 2nd-order accurate and the polynomial reconstruction in the solver allows a selection between centroidal-based and nodal-based polynomials. In the present work, most of the computations were performed using the centroidal-based polynomials. Time integration uses an implicit method.

Figure 2 shows the  $C_L$  versus angle-of-attack ( $AoA$ ) curves obtained by the simulations performed with the turbulence models considered in this study. One can observe that the results obtained with the LM model are close to those obtained with the cubic  $k - \epsilon$  model. Both results show the same stall angle-of-attack and the maximum lift coefficient. It is interesting to notice that the LM and the SST model are in accordance for the lift coefficient up to 28 deg. Beyond this angle-of-attack the LM model is still indicating a raise in the lift coefficient whilst the SST model presents a decrease in the lift coefficient.

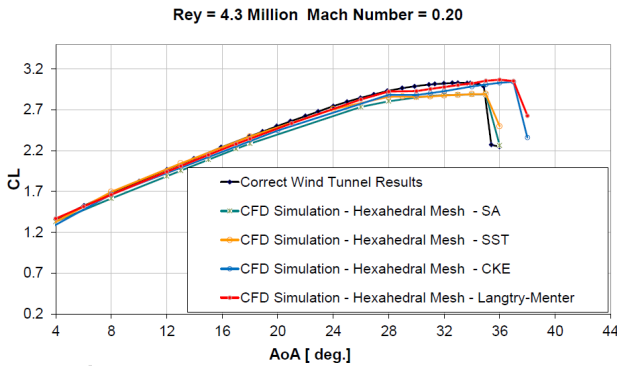


**Fig. 2** Lift coefficient curves for the different turbulence models addressed in this paper.

One could expect the results of the LM transition model to be close to those obtained with the original SST turbulence model. A possible explanation for the observed discrepancies between the results of these two models can be found in the fact that, by using the LM model, each wing element presents a laminar flow region. The first stages of the boundary layer development impact on the overall boundary layer evolution given the parabolic nature of the boundary layer physics in the streamwise direction. As a result,

a boundary layer that is laminar close to the leading edge can lead to distinct aerodynamic coefficients when compared to a fully-turbulent boundary layer. Another effect that could be even more relevant than the boundary layer history effects is the distinct separated flow topologies when different models are used. Indeed, the boundary layer is strongly affected by the inviscid flow pressure gradient, which is, in turn, influenced by the presence of separated flow regions.

Figure 3 illustrates the numerical results obtained with the SST and the LM turbulence models for the breakdown of the lift coefficient for each component of the wing. It is possible to observe that, for the angles of attack above 28 deg., the main element is the one that mostly contributes for the difference in the  $C_L$  between the SST and LM model results. The comparison of the lift coefficient results, for the slat and flap components, indicates that the calculations with the two different models yield quite similar values of  $C_L$  in almost the entire range of angle-of-attack.

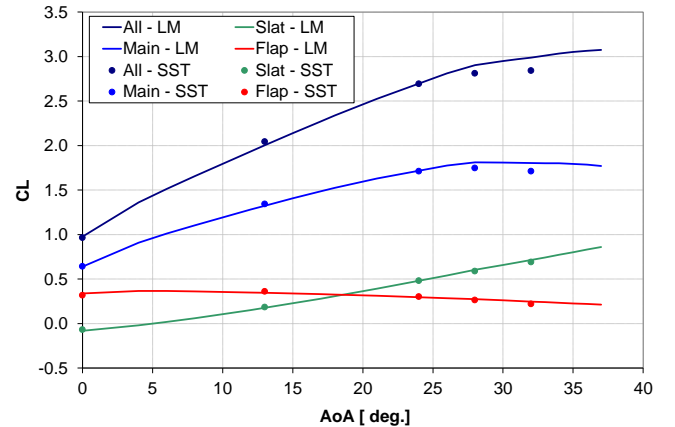


**Fig. 3** Lift coefficient for the three wing components – SST and LM turbulence models.

Although both models yield similar values for the lift coefficient in the range between 0 and 28 deg. of angle-of-attack, the flow pattern is different for almost the entire range of  $AoA$  considered. Figures 4 and 5 show the friction coefficient,  $C_f$ , and the shear lines over the components of configuration “one” for  $AoA = 13$  deg. It is possi-

ble to notice for this specific angle-of-attack that the LM model results indicate a separation bubble in the outer part of the slat panel and, also, a flow detachment region at the trailing edge of this component. Moreover, the results for the LM model also indicate a quite extensive flow separation over the flap component, as one can see in Fig. 5.

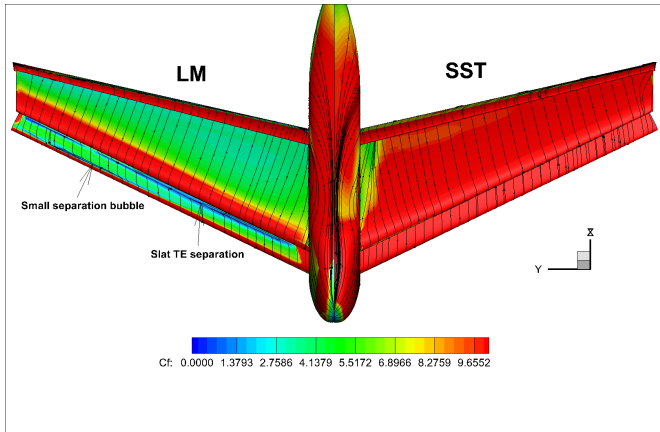


**Fig. 4** Shear lines and skin friction coefficient contours over configuration *one* for the SST and the Langtry-Menter models for  $AoA = 13$  deg.

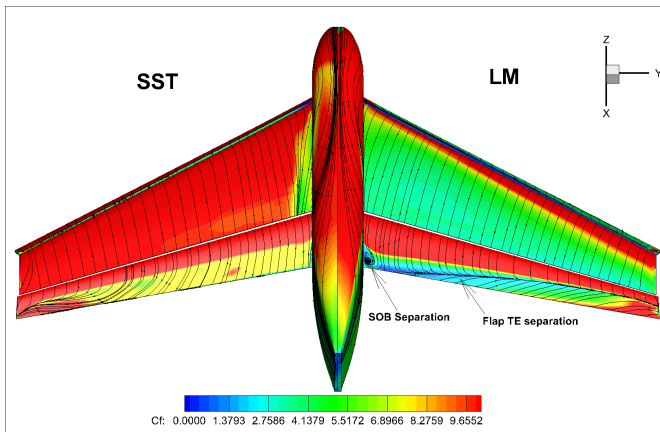


**Fig. 5** Shear lines and skin friction coefficient contours over configuration *one* for the SST and the Langtry-Menter models at  $AoA = 13$  deg. with emphasis on the flap flowfield.

These separation regions are also identified in Figs. 6 and 7. These two figures show, respectively, the pressure coefficient distribution over

the slat and flap components at an extracted station slice located at  $\eta = 0.65$  of the HLP spanwise direction. Figure 6 shows the two flow separation regions for the slat component. As discussed, the results for the LM model also show that there is flow separation over the upper surface of the flap component, as indicated in Fig. 7.

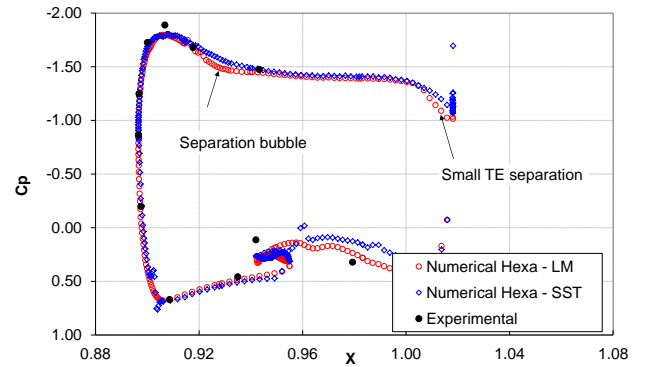


**Fig. 6** Pressure coefficient distribution over the slat for  $\eta = 0.65$  and  $AoA = 13$  deg.

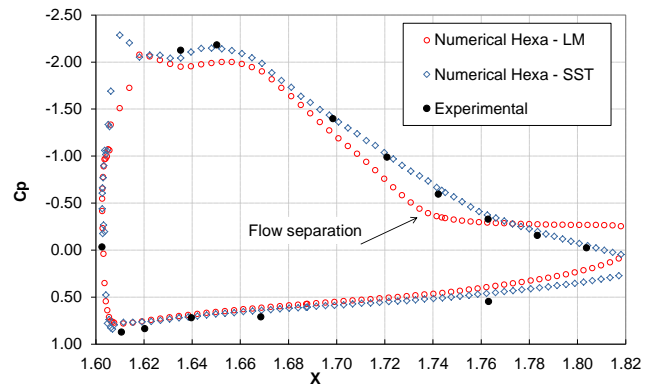


**Fig. 7** Pressure coefficient distribution over the flap for  $\eta = 0.65$  and  $AoA = 13$  deg.

The results with the LM turbulence model yield considerable flow separation region over the flap panel. The increase in the angle-of-attack causes a small movement of the detachment line in the upstream direction until an  $AoA$  of 28 deg. For  $AoA$  values above 28 deg., the results begin to show a decrease in the detached region in the

outboard flap panel, as one can observe in Fig. 8.

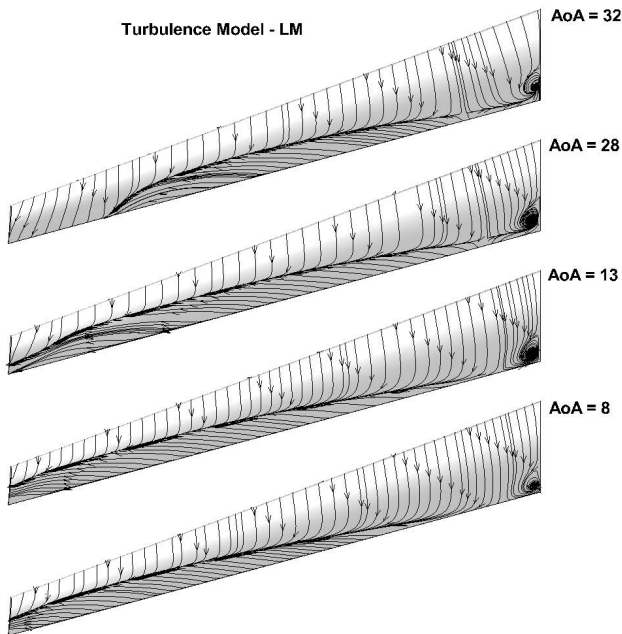


**Fig. 8** Shear lines over the flap panel for  $AoA = 8, 13, 24$  and  $32$  deg.

Figure 9 shows that the flow pattern obtained with the SST turbulence model over the flap component. From such figure, it is clear that there is no massive flow separation region for the results with the SST model. It is possible that the side-of-body separation observed in the simulations with the Langtry-Menter model might be inducing a very different flow pattern over the flap, which justifies such large differences between the two sets of results. However, this observation must be further investigated before a more definite conclusion could be reached on the reasons for such large differences between the simulations with the two different models.

It is clear that the differences in flow pattern would certainly affect the drag calculations. Hence, despite the similarity from SST and LM results for the lift coefficient values, the obtained data for the drag coefficient is considerably distinct, as one can observe in Fig. 10. The Langtry-Menter model leads to a lower drag coefficient for the entire range of lift coefficients. In part,

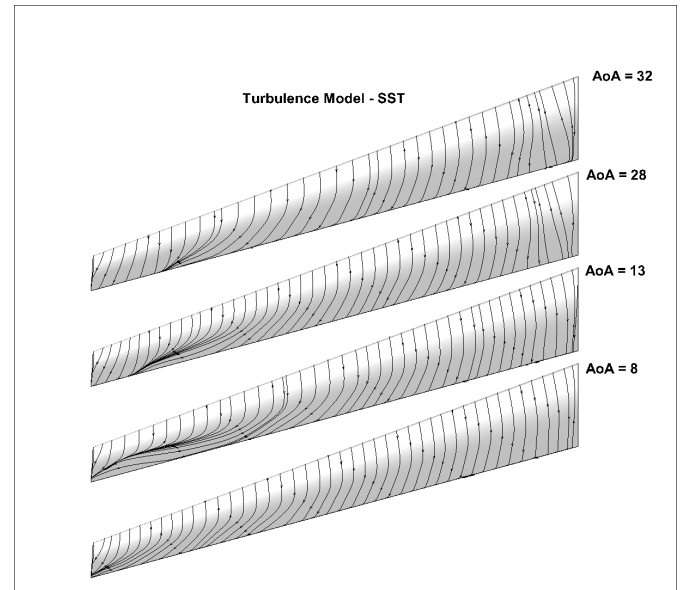


**Fig. 9** Shear lines over the flap panel for  $AoA = 8, 13, 24$  and  $32$  deg.

this difference could be attributed to the laminar flow regions over the aerodynamic components. Figure 11 provides a general overview of the skin friction coefficient,  $C_f$ , for both solutions. It is possible to observe the existence of a much lower skin friction contribution from the LM model results with respect to those obtained with the SST model. Definitely, these differences have some contribution in the computation of the total drag coefficient.

The drag coefficient evolution with the angle-of-attack for the slat is shown in Fig. 12. One can observe that the pressure distribution for the slat component is the most favorable among all the elements to sustain a large extension of a laminar region of the flow, which is explained by the fact that Tollmien-Schlichting waves are stabilized by favorable pressure gradients [9]. Thereby, it is in this component that most of the difference in the drag coefficient should be noticed for the SST and the LM models. It is important to observe that on such device the drag force is pointing forward which means a negative drag. The obtained results indicate that the LM model yields a lower drag coefficient with the increase of the angle-of-attack. This is a consequence of the reattachment

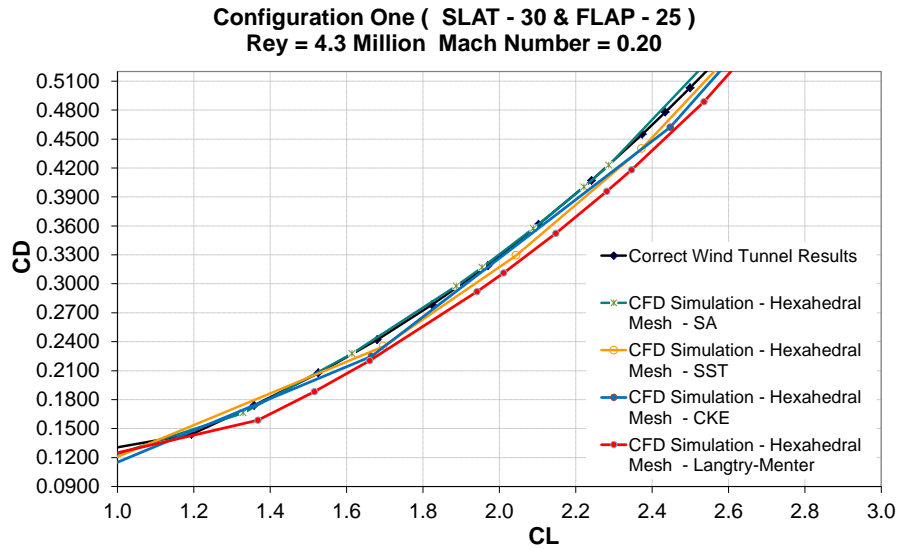


**Fig. 10** Drag polars for the different turbulence models addressed in this paper.

of the flowfield at the slat trailing edge.

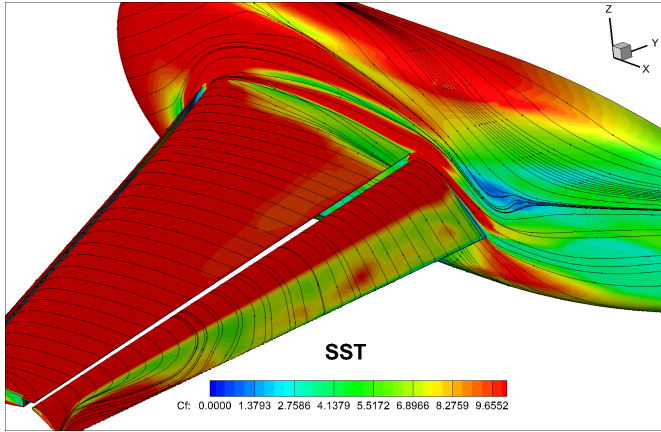
Figure 13 shows a similar comparison between the turbulence models for the drag coefficient but, in this case, for the main element. The LM model shows a higher drag coefficient as the angle-of-attack increases beyond 28 deg. which is the opposite trend to the one observed in the slat component. The increase in the drag coefficient with the  $AoA$  can be seen as a consequence of the fact that the main element is more aerodynamically loaded than the slat itself.

The drag coefficient curves for the flap are illustrated in Fig. 14, again for both LM and SST models. It is observed that the calculations with the SST model lead to higher drag coefficient values for angles-of-attack up to 25 deg. As depicted in Figs. 4 and 5, the calculations with the LM model yield separated flow regions for this angle-of-attack range, which are not present in the SST numerical results. This behavior is, therefore, strange because one would expect that the benefits of having a laminar region should not be able to compensate the increase in the total pressure drag due to flow separation. The expectation would be that the pressure drag increases in such detached flow regions would overcome the friction drag reduction due to laminar flow in the

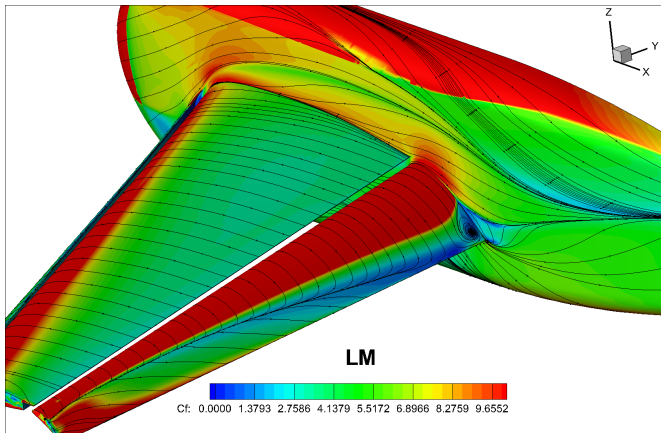
LM model. Therefore, it is clear that the current results still need to be further investigated in order to understand why such behavior was observed. Ongoing research aims at providing better insights on such behavior.

The results obtained with the current investigation could, then, be summarized by stating that the Langtry-Menter model has led to a lower overall drag coefficient for the entire range of lift coefficients analyzed here. This result can be explained, at least partially, due to the laminar flow region over the aerodynamic components provided by the solution with this model. The behavior, however, is somewhat unexpected since the regions of separated flow predicted by the LM model over some of the wing components should, in principle, lead to large pressure drag coefficients. Moreover, an analysis of drag contributions indicates that the pressure drag is quite larger than the contributions that come from friction drag. Hence, the expectation would be that the large values of pressure drag would overcome, in general, the viscous drag for separated flows. Therefore, one would expect that, even with the reduced skin friction drag related to the initial laminar regions predicted by the LM model, the overall resulting drag would

## EFFECTS OF TRANSITION ON THE GLOBAL AERODYNAMIC COEFFICIENTS



(a) SST Turbulence Model.



(b) LM Transition Model.

**Fig. 11** Skin friction coefficient contours for the SST and LM turbulence models

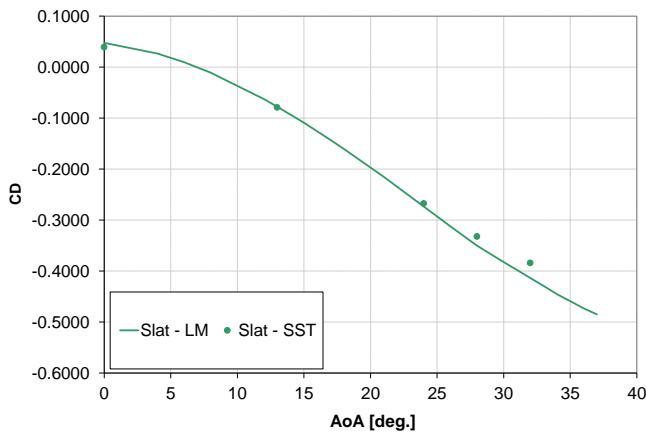


**Fig. 12** Drag coefficient as obtained with the SST and LM models – slat component.

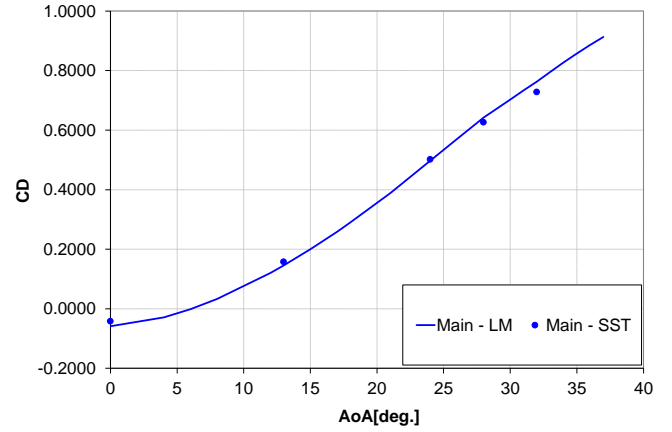


**Fig. 13** Drag coefficient as obtained with the SST and LM models – main component.

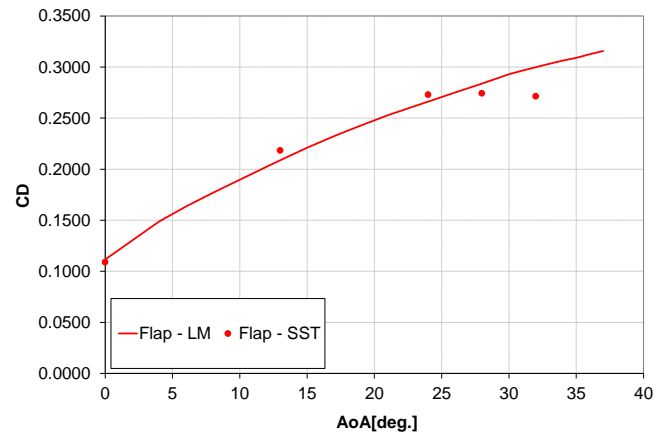


**Fig. 14** Drag coefficient as obtained with the SST and LM models – flap component.

present larger values for the LM model results when compared to those obtained with the SST model.

### 4 Concluding Remarks

Transition to turbulence is an important phenomenon in aerodynamics. It is widely known that laminar and turbulent flows present distinct behavior, with relevant impacts in several practical engineering applications. In the present paper, the impacts of transition to turbulence in the aerodynamic coefficients of a high-lift configuration are addressed. Simulations are per-

formed using the Shear Stress Transport (SST) turbulence model, as the base turbulence closure procedure, and comparisons are made considering the inclusion, or not, of the Langtry-Menter (LM) transition model. It is observed that the inclusion of the transition effects, by means of the LM model, leads to numerical results that are quite different from those obtained using solely the underlying turbulence closure, namely, the SST model.

In the linear part of the lift coefficient curve, all models present similar trends, but the inclusion of the transition model leads to a better agreement with wind tunnel data. Actually, the lift curve results for this case are very similar to those obtained with the cubic  $k - \epsilon$  model. In the nonlinear portion of the lift coefficient curve, as a function of angle-of-attack, no model can correctly reproduce the experimental data. In particular, the results with the LM model are the ones that best fit the experimental data, even though the stall angle-of-attack is not correctly recovered.

Analyses of flow topologies and pressure coefficient distributions at some spanwise stations indicate that the results obtained with the SST model augmented by the LM transition model have separation bubbles and detached flow regions, both along the slat and the flap, for most of the angle-of-attack range analyzed. This is in contrast with the results obtained simply with the SST model, which do not show such flow separation regions. The differences in flow topology can certainly be explained by the fact that, with the transition model, there are certain portions of the flow over the wing which can be laminar. Therefore, these regions are more prone to flow separation. Furthermore, the distinct pressure distributions, which present a considerable influence on the boundary layer evolution, can also be seen as a cause of such different flow topologies.

The results which were unexpected, however, were those associated to the drag coefficient. The calculations with the Langtry-Menter model have led to a lower overall drag coefficient for the entire range of lift coefficients analyzed

here. Such behavior is somewhat unexpected because the regions of separated flow predicted by the LM model, over some of the wing components, should, in principle, lead to large pressure drag coefficients. The pressure drag contributions are much larger than the contributions that come from friction drag. Hence, the expected result would be that the large values of pressure drag would overcome the viscous drag for separated flows. Therefore, one would expect that, even with the reduced skin friction drag related to the initial laminar regions predicted by the LM model, the overall resulting drag would present larger values for the LM model results when compared to those obtained with the SST model. At the time of this writing, there is ongoing research that is directed at providing better insights on such behavior.

### Acknowledgments

The authors gratefully acknowledge the support for the present research provided by Conselho Nacional de Desenvolvimento Científico e Tecnológico, CNPq, under the Research Grants No. 309985/2013-7, No. 400844/2014-1 and No. 443839/2014-0. The work is also supported by Fundação de Amparo à Pesquisa do Estado de São Paulo, FAPESP, under the Research Grants No. 2008/57866-1 and No. 2013/07375-0.

### References

- [1] Metacomp Technologies Inc., CFD++, "<http://www.metacomptech.com/>".
- [2] Langtry, R. B., and Menter, F. R., "Correlation-Based Transition Modeling for Unstructured Parallelized Computational Fluid Dynamics Codes," *AIAA Journal*, Vol. 47, No. 12, Dec. 2009, pp. 2894–2906.
- [3] Antunes, A. P., Azevedo, J. L. F., and da Silva, R. G., "Numerical Simulations of Turbulent Flow over a High-Lift Configuration," AIAA Paper No. 2011-3006, *Proceedings of the 29th AIAA Applied Aerodynamics Conference*, Honolulu, HI, June 2011.
- [4] Spalart, P. R., and Allmaras, S. R., "A One-Equation Turbulence Model for Aerodynamic

- Flows,” AIAA Paper No. 92-0439, *30th AIAA Aerospace Sciences Meeting and Exhibit*, Reno, NV, Jan. 1992.
- [5] Menter, F. R., “Two-Equation Eddy-Viscosity Turbulence Models for Engineering Applications,” *AIAA Journal*, Vol. 32, No. 8, Aug. 1993, pp. 1598–1605.
- [6] Ansys Inc., ICEM-CFD™, “<http://www.icemcfd.com/>”.
- [7] Menter, F. R., “Two-Equation Eddy Viscosity Turbulence Models for Engineering Applications,” *AIAA Journal*, Vol. 32, No. 8, Feb. 1994, pp. 1598–1605.
- [8] Langtry, R. B., *A Correlation-Based Transition Modeling using Local Variables for Unstructured Parallelized CFD Codes*, Ph.D. Thesis, Universität Stuttgart, Stuttgart, Germany, 2006.
- [9] Halila, G. L. O., *A Numerical Study on Transitional Flows by Means of a Correlation-Based Transition Model*, M.Eng. Thesis, Instituto Tecnológico de Aeronáutica, São José dos Campos, SP, Brazil, 2014.

### 5 Contact Author Email Addresses

G. O. L. Halila, [gustavo.halila@embraer.com.br](mailto:gustavo.halila@embraer.com.br)  
A. P. Antunes, [alexandre.antunes@embraer.com.br](mailto:alexandre.antunes@embraer.com.br)  
R. G. da Silva, [ri\\_galdino@yahoo.com.br](mailto:ri_galdino@yahoo.com.br)  
J. L. F. Azevedo, [joaoluiz.azevedo@gmail.com](mailto:joaoluiz.azevedo@gmail.com)

### Copyright Statement

The authors confirm that they, and/or their company or organization, hold copyright on all of the original material included in this paper. The authors also confirm that they have obtained permission, from the copyright holder of any third party material included in this paper, to publish it as part of their paper. The authors confirm that they give permission, or have obtained permission from the copyright holder of this paper, for the publication and distribution of this paper as part of the ICAS 2016 proceedings or as individual off-prints from the proceedings.